

On the Relation Between the Large-Scale Tropospheric Circulation and Air Quality in Tehran

Hafezi, M.¹, Mohebalhojeh, A. R.^{2*}, Aliakbari-Bidokhti, A. A.³, Irannejad, P.², Sabetghadam, S.⁴

1. Ph.D. Student, Department of Space Physics, Institute of Geophysics, University of Tehran, Iran
2. Associate Professor, Department of Space Physics, Institute of Geophysics, University of Tehran, Iran
3. Professor, Department of Space Physics, Institute of Geophysics, University of Tehran, Iran
4. Assistant Professor, Department of Space Physics, Institute of Geophysics, University of Tehran, Iran

(Received: 29 May 2017, Accepted: 24 Oct 2017)

Abstract

The large-scale tropospheric circulation can play a controlling role in the accumulation and ventilation of air pollutants. It thus impacts air quality in large urban areas. This paper investigates the statistical relations between the dynamical indices related to circulation in the troposphere and visibility as a surrogate for air pollution in the urban area of Tehran for the climatological period of 1958 to 2013. The dynamical indices are based on jet splitting and Rossby wave breaking at the upper troposphere, eddy kinetic energy, meridional momentum flux, and static stability at the lower troposphere, as well as the high and low surface pressure disturbances. Despite the definite impact of surface pressure disturbances on visibility in Tehran, results show only very weak, if any, relation between the tropospheric circulation indices and visibility in Tehran. The absence of a robust relation is attributed to the slow response of the urban ventilation process to the time evolution of dynamical indices above the boundary layer and particularly at upper troposphere. The complex terrain of the region is likely the main factor creating the slow response.

Keywords: Tehran, Air pollution episodes, Dynamical indices, Blocking, Split flow.

1. Introduction

Air pollution is produced from both natural and anthropogenic sources (Seinfeld and Pandis, 2006). It has been found to be associated with a wide range of adverse health effects (Samet and Krewski, 2007) as well as impaired visibility, which is a problem for traffic safety (Sisler and Malm, 1994). As the concentration of pollutants could be affected by various meteorological factors (Pearce et al., 2011), the long term evaluation of the air quality is also important to understand the potential impact of climate change (Mickley et al., 2004).

In the absence of certain weather conditions (e.g., fog and rain), visibility could be used as an indicator of air quality (Baumer et al., 2008). Many researchers have examined the observed visibility and its connection with local air pollution over the globe (for example, Husar et al., 1981; Doyle and Dorling, 2002; Deng et al., 2008; Chang et al., 2009; Sabetghadam et al., 2012; Xiao et al., 2014). Low level meteorological variables such as relative humidity, temperature, wind velocity and direction can directly affect air pollution (Molenaar et al., 2008; Gulpepe and Milbrandt,

2009; Pusheng et al., 2011; Dagsson-Waldhauserova et al., 2013; Liao et al., 2015). Apart from meteorological factors, some dynamical events with varying scales from large to meso could affect the concentration of air pollution (Shen and Mickley, 2017). Simulations by General Circulation Models (GCM) show that the increasing concentration of greenhouse gases contributes to a poleward shift in the position of subtropical jet stream and storm tracks, a decrease in the frequency, but an increase in intensity of the Northern Hemisphere midlatitude cyclones (Lambert and Fyfe, 2006; Meehl et al., 2007). A reduction in the frequency of mid latitude cyclones may lead to fewer cold fronts passing through the polluted regions, causing a higher frequency of stagnation periods (Mickley et al., 2004; Forkel and Knoche, 2006; Murazaki and Hess, 2006; Wu et al., 2008).

Changes in the large-scale circulation associated with global warming are expected to change the intensity and frequency of occurrence of acute air pollution events. The cold fronts accompanying mid-latitude

*Corresponding author:

amoheb@ut.ac.ir

cyclones have been identified as the key factor for air pollution ventilation in western North America, Europe and East Asia (Cooper et al., 2001; Liu et al., 2003; Li et al., 2005; Ordonez et al., 2005). Tai et al. (2012) demonstrated the cold front passage as the prominent meteorological process involved in variation of PM_{2.5} in the eastern US. Frequency of mid-latitude cyclones has been used as a predictor of stagnation and ozone pollution days in the eastern US (Leibensperger et al., 2008). With their potential to affect the air quality and visual range, the surface high-pressure and low-pressure systems are among the mesoscale weather disturbances that need to be investigated.

With its growing population and industrialization, the megacity of Tehran is prone to high episodes of unhealthy days, especially in the cold season. Even in case of no or little interannual change in local emission of pollutants, there is an important degree of variability in the statistics of hazardous air pollution episodes in Tehran. The statistics such as the frequency of occurrence and intensity are expected to change during the next couple of decades with regional impacts of global warming, even in case of a stationary state for the local emission in the megacity. As a step toward understanding the impact of climate change on air quality in Tehran, this paper aims to investigate the possible links between the air pollution in Tehran and certain dynamical indices of large-scale flow; including the split flow, blocking, eddy kinetic energy and meridional momentum flux. The link with the surface high and low pressure disturbances is also investigated. Precedence to this work goes to Hafezi et al. (2015) which showed that some sub-episodes of air pollution in the acute and air pollution period occurred in Nov–Dec 2010 in Tehran were related to the formation of an instantaneous blocking in central Asia accompanied with jet splitting that is quantified by the split flow index. Being limited to a case study, the usefulness or otherwise of such indices in a statistical sense remains to be examined. Further, there is a general interest in the relation between the tropospheric circulation and local air quality for its possible use in downscaling the general circulation and global climate model results for air quality purposes (e.g., Rohli et al., 2004; Demuzere et al., 2009; Dharshana et al., 2010;

Pope et al., 2014; Pope et al., 2015; Webber et al., 2017).

The paper is structured as follows: The different datasets used and the methodology employed in defining the dynamical indices are described in Section 2. In the absence of long-term records of air pollution in the area of study, the visibility data are used as indicators of air quality. In the third section, results are presented for the statistics of the relation between the dynamical indices and the visibility impairment. In the final section, the main conclusions are given.

2. Data and methodology

2.1. Data

Geographically surrounded from north by Alborz mountain ranges, from south by Kavir desert, and from west to southwest by low-elevated land, Tehran is approximately located from 51°2'E to 51°36'E in longitude and from 35°34'N to 35°50'N in latitude. Besides this specific location, the highly populated and industrialized urban area of Tehran provides ground for frequent visibility impairment episodes due to the acute air pollution especially in cold seasons.

In this study, two types of data are used. The first is visibility observations as carried out in three-hourly intervals in Tehran Mehrabad Airport synoptic station, located 1190.8 m above mean sea level at 35°41'N/51°19'E. This station is the only site in Tehran Province with more than 50 years of continuous synoptic data. The second type is the sea surface pressure, zonal and meridional components of wind and air temperature in six hourly intervals for the period 1958–2013 as obtained from the National Centers for Environmental Prediction–National Center for Atmospheric Research, usually called NCEP/NCAR, reanalysis dataset (Kalnay et al., 1996). The six-hourly synoptic patterns of the surface pressure in a domain covering 24°–40° N, 44°–64° E were investigated. For a rectangular latitude–longitude subdomain (34°–37° N, 48°–54° N), centered at Tehran, the frequency of occurrence was determined for the surface pressure disturbances. To identify the low (high) pressure disturbances, the grid-point values of the surface pressure were

probed to find cases where the pressure in a given grid point was lower (higher) than its surrounding grid points with distances of no greater than about 240 km.

As mentioned in the introduction, due to the relation between visibility and the concentration of particulate matter as the main cause of acute air pollution, screening the visibility dataset is required to eliminate the effects of weather on visual range. As shown by Malm and Day (2001), the increase in relative humidity levels will substantially increase the light scattering cross section of ammonium sulfate particles relative to that of dry particles, which can directly influence visual range. For this reason, many previous studies on atmospheric visibility have screened observations of visibility when relative humidity is greater than 90% (e.g., Craig and Faulkenberry, 1979; Doyle and Dorling, 2002). The meteorological filter has been used in a way to remove all cases of fog, precipitation and relative humidity higher than 70%. For both the filtered and unfiltered (raw) observations, the daily averages and cumulative percentiles (Sloane, 1982a, b, 1984; Deng et al., 2012; Xiao et al., 2014) were obtained. The i^{th} cumulative percentile is the visibility that equals or exceeds i percent of the time.

2.2. The split flow index

The use of dynamical indices facilitates the quest for the links between large-scale atmospheric events and local air pollution episodes. Among such indices is the ‘‘Split Flow Index’’ or SFI in brief, defined by:

$$\text{SFI} = \zeta_{\text{STJ}} + \zeta_{\text{PFJ}} - \zeta_{\text{GAP}}, \quad (1)$$

which serves to study the influence of strength and location of two main jet streams in the upper troposphere on a given region (Bals-Elsholz et al., 2001). In Equation (1), ζ_{GAP} , ζ_{STJ} and ζ_{PFJ} are the average vertical component of relative vorticity of the GAP, STJ and PFJ regions at 200 hPa level. The GAP is defined to represent the region with minimum wind speed and activity between the regions occupied by the subtropical jet stream, denoted by STJ, and the polar jet stream denoted by PFJ. The relative location of each jet and GAP has been defined by referring to the effect of jet splitting

on some acute air pollution and clean air episodes. As determined based on the acute air pollution events, the STJ, GAP and PFJ locations are respectively 13° – 28° N, 34° – 50° N and 55° – 70° N. In order to reach a trade-off between the large-scale structure of jet splitting and its probable microscale effects on the surface, the SFI values have been computed and averaged over a longitudinal band from 45° E to 60° E. Further, the resulting daily values of the SFI have been normalized by subtracting from the monthly mean and then dividing the result by the standard deviation of the SFI. As determined, the positive and negative values imply the presence of split and non-split flows, respectively. Note that this is the opposite of the situation in the Southern Hemisphere studied by Bals-Elsholz et al. (2001) because of the change in sign of vertical component of vorticity between the two hemispheres. The formation of split flow in upstream and a distinct gap region over Tehran are expected to provide adverse conditions for air quality in Tehran. This is the basis of using positive values of the SFI as a precursor for the occurrence of acute air pollution events. It should be mentioned that the computation of the relative vorticity field has been carried out using spherical harmonics by the subroutines provided in the SPHEREPACK 3.0 (Adams and Swarztrauber, 1999).

2.3. The Rossby wave breaking index

As arguably the most fundamental dynamical quantity combining the effects of both rotation and stratification, Potential Vorticity (PV) provides great facility in understanding a large spectrum of atmospheric flows (Hoskins et al., 1985; Haynes and McIntyre, 1987; Thorncroft et al., 1993). Among such flows are the breaking, large-amplitude Rossby waves involved in large-scale blocking events. The adverse positioning of the ridge or the closed regions of high geopotential height at pressure surfaces during blocking episodes with their potential to stagnate is usually responsible for the cases of extreme air pollution. In recent decades, attempts have been made to use PV diagnostics for introducing suitable indices based on Rossby-wave breaking to detect and

quantify the blocking formation. Based on the distribution of meridional gradient of potential temperature θ on “2 PV unit” surface, usually denoted by 2PVU for $10^{-6} \text{ m}^2 \text{ s}^{-1} \text{ K kg}^{-1}$ being the PV unit, Pelly and Hoskins (2003) introduced an index for wave breaking. This index has recently been used by Webber et al. (2017) to determine the impact of Rossby wave breaking on the concentration of PM_{10} in the UK. The index is called B and defined by:

$$B = \frac{2}{\Delta\varphi} \left(\int_{\varphi_0}^{\varphi_0 + \Delta\varphi/2} \theta \, d\varphi - \int_{\varphi_0 - \Delta\varphi/2}^{\varphi_0} \theta \, d\varphi \right), \quad (2)$$

where φ_0 is the blocking latitude, $\Delta\varphi$ is a typical scale of blocking width taken to be 30° . To calculate φ_0 , the transient eddy kinetic energy associated with the baroclinic eddies for each month of the study proves helpful to define the average value of the central blocking latitude (φ_c):

$$\varphi_0 = \varphi_c(\lambda) \pm \Delta, \quad (3)$$

which is longitude dependent. The Δ in Equation (3) is taken to be 4° . To determine φ_c , the eddy kinetic energy of the transient eddies (K), as defined shortly, is computed and averaged vertically from 100 hPa to 500 hPa. As in Pelly and Hoskins (2003), φ_c is taken to be the latitude at which K becomes maximum. The blocking index B is then set to the maximum value obtained from Equation (2) for the three values of φ_0 given by Equation (3). The spatio-temporal structure of the positive values of B is associated with the occurrence of blocking events of varying longitudinal extent and time span from local instantaneous to large-scale persistent cases. For an application to the problem of air pollution in Tehran, we seek the possible link between Tehran’s visibility and the daily values of the B index averaged over 50° E and 52.5° E as the adverse positions of the blocking events.

2.4. The eddy kinetic energy and relatives

Defined by $K = (u'^2 + v'^2) / 2$ with u' and

v' denoting the band-pass filtered zonal and meridional velocity components, respectively, the eddy kinetic energy provides a useful measure of synoptic-scale activity (Chang et al., 2002). The band-pass filtering is carried out using the Lanczos filter (Duchon, 1979) to retain periods between two and ten days related to high-frequency eddies. It is expected that the higher levels of synoptic-scale activity in the lower troposphere can help the ventilation process and thus play a role in reducing air pollution and increasing the visibility. However, as defined, K treats equally the downstream and upstream sides of the troughs of the geopotential height field where, respectively, ascending and descending motions are expected. As a way of differentiating the K values in different regions of a synoptic-scale wave, two other dynamical quantities of $K_{\text{mf}} = K \times \text{sgn}(MF)$ and $K_s = K \times (-S)$ with $MF = u'v'$ representing the northward meridional momentum flux, S the static stability, and sgn the sign function were defined. Both momentum flux and static stability change behavior from upstream to downstream side of a trough. Further, the lower tropospheric stability is expected to be directly linked with the changes in the boundary-layer processes and thus the changes in air pollution. Therefore, for completeness, MF and S are also assessed in addition to K , K_{mf} and K_s in our quest to find dynamical links with the visibility. Results presented for the eddy kinetic energy and meridional momentum flux are for the 850 hPa level and those for the static stability are for the 800 hPa level.

3. Results and analysis

3.1. The role of dynamical indices

From climatological point of view, taking the monthly average values of the SFI and the B index would result in the loss of sub-monthly details. Consistent with synoptic patterns, the acute air pollution and visibility degradation episodes are expected to have weekly time scales. The shortest time scale to investigate the link between large-scale dynamical indices and the local changes in

the visibility is that of daily time scale. Therefore, the daily and five-day averages were used for the analysis. With regard to the closeness of the results for the daily and five-day averages, for the sake of brevity, here, only results for the daily averages are reported. The negative linear trend evidently present in the average values of the screened visibility observations for the winter season, Dec. to Feb. called DJF, as seen in Figure 1 makes de-trending of the visibility data necessary. This was carried out by simply subtracting the linear trend from the average values. However, neither the SFI nor the B index showed any specific trend for the same period and therefore no de-trending was required. The scatter plots of the SFI and the B index show that most of the data points are accumulated around the mean value and to extract meaningful information from the data, a categorization of the data is necessary. By using the threshold values of ± 0.5 , the SFI is categorized into three groups with (i) $\text{SFI} < -0.5$, (ii) $-0.5 < \text{SFI} < 0.5$ and (iii) $\text{SFI} > 0.5$. Having a nonzero mean value, the B index is categorized in a different manner. For each month, the two limits are taken to be the median of the B plus/minus its standard deviation and the three groups of data are constructed in the same way as those of the SFI.

We start with testing the null hypothesis of independence of the two indices and visibility using the chi-squared test:

$$\chi^2 = \sum_i \frac{(O_i - E_i)^2}{E_i}, \quad (4)$$

where O_i and E_i are, respectively, the observed and expected numbers of cases in each cell of the contingency table. As a rule, if the chi-squared statistic exceeds the critical chi-squared value at 0.05 significance level, then the null hypothesis is rejected and the alternative hypothesis of the existence of a relationship between the two variables is accepted. To carry out the test, for the de-trended and screened visibility observations, the first (0.25) and third (0.75) quartiles were calculated. For the SFI and the B index, the frequencies of occurrence were calculated for each of their three groups of data. A similar procedure was applied to the rest of the

indices. Then a 3×3 contingency table was formed for each index, which helps to calculate the chi-squared test of independence. Based on the results presented in Table 1, disregarding the month of February for the SFI, the chi-squared test values for the SFI, B , K , K_{mf} and MF at all four months are smaller than 9.488, the chi-squared value for 4 degrees of freedom and p -value of 0.05. This indicates that the null hypothesis of independence of the two indices from the visibility cannot be rejected. However, for K_S and S , at each of the four months, the null hypothesis of independence is rejected.

Table 1. The χ^2 statistics for dynamical quantities defined in the text and tested against de-trended visibilities. The starred values are those for which the hypothesis of no association is rejected. Visibility observations and NCEP-NCAR reanalysis data have been used for χ^2 statistics computation.

Quantity	Nov.	Dec.	Jan.	Feb.
SFI	9.37	4.7	4.82	9.99*
B	5.59	3.48	>10*	2.84
K	7.32	8.36	2.02	3.61
K_{mf}	7.79	9.4	4.44	1.45
K_S	9.84*	12.95*	>14*	>12*
MF	7.58	5.56	3	0.56
S	11.1*	24.66*	>13*	>11*

Despite the strong negative results from the chi-squared test for most of the indices and the smallness of the correlation values in Table 2, the quest for finding any possible relation is continued by looking into the probabilities of visibility exceeding certain threshold under the condition of the indices taking their small or large values. To this end, the following three-step procedure is carried out for each index:

1. In the first step, a threshold is determined for each year and month, then the frequency of occurrence is determined for values smaller than the threshold. To this end, the third (0.75) quartile of the general index X is determined and regarded as the threshold of X that is denoted by X_{th} . Then for year Y and month M of the study, the frequency of occurrence for $X < X_{th}$ is

determined and denoted by $N(X, Y, M)$.

2. For the 56 values of the variable $N(X, Y, M)$, the first (0.25) quartile of N is determined and called $N_{0.25}(X, M)$. This number determines a low value for the frequencies of occurrence to be used in the next step.

3. The years for which $N(X, Y, M) > N_{0.25}(X, M)$ constitute a set called $A_{0.25}(X, M)$. This set has N_Y members and is a function of X and M . Conceptually, the set $A_{0.25}(X, M)$ includes the years for which the frequency of occurrence of smaller than the threshold values of the quantity X is not small. By implication, it can give us a way to measure the impact of large values of X . A slightly different procedure was applied to determine the threshold for the visibility, called V_{th} by counting the cases of the visibility under the specific value defined for each year and month according to:

$$V_{th} = \frac{\bar{V}_{90}(M)}{\bar{V}(Y, M)} \times \bar{V}(M), \quad (5)$$

in which $\bar{V}_{90}(M)$ is the 56 year average of 90th percentile visibility for the month M , $\bar{V}(Y, M)$ is the average visibility for the month M in the year Y , and $\bar{V}(M)$ is the 56 year average visibility. By using Equation (5), a variable threshold will be obtained for a month of each year and the values under the specific threshold will be counted. Following what described for the general index X , $N_Y(V, M)$ and $A_{0.25}(V, M)$ are determined for the visibility data. As constructed, the set $A_{0.25}(V, M)$ includes the years for which the frequency of occurrence of poor visibility is not small. The conditional probability is then computed using:

$$p(V | X) = \frac{p(X, V)}{p(X)}, \quad (6)$$

Where

$$p(X) = N_Y(X, M) / N_{tot}, \quad p(V) = N_Y(V, M) / N_{tot}, \\ p(X, V) = N_Y(X, V, M) / N_{tot} \text{ with } N_{tot} \text{ the}$$

number of years used in the probability estimation and $N_Y(X, V, M)$ the number of years shared between the two statistical sets of $A_{0.25}(X, M)$ and $A_{0.25}(V, M)$.

Based on the procedure described above, given in Table 3 are $p(V | X) - p(V)$ for X taken to be the SFI, B , K , K_{mf} , K_S , MF , S as well as F_{high} and F_{low} representing the frequencies of occurrence for, respectively, the high- and low-pressure systems. The sign-definite changes across the four months are due to B , F_{high} and F_{low} .

The positive values of F_{high} are consistent with the increase in probability of a given year to have large number of days with poor visibility, when the number of days with high-pressure is large. A similar argument can be made for F_{low} , i.e. for the number of days with low-pressure systems, which have the opposite effect on the visibility. The greatest discernible effect, between 6% and 16% in magnitude, is that of F_{low} . For the rest of the dynamical variables, no definite conclusion can be made across the season.

Table 2. The correlation between the daily values of the dynamical quantities defined in the text (given from NCEP-NCAR reanalysis quantities) and the daily de-trended visibility (given from Mehrabad Airport synoptic station). The starred and doubly-starred values refer to those with statistical significance at 0.05 and 0.01 levels, respectively.

Quantity X	Nov.	Dec.	Jan.	Feb.
SFI	-0.06*	-0.01	0.05*	0.06*
B	0.02	-0.03	0.11**	0.02
K	0.05*	0.07*	0.02	0.01
K_{mf}	0.01	0.04	-0.07*	-0.03
K_S	0.01	0.11**	0.16**	0.12**
MF	0.01	0.06*	-0.06*	-0.03
S	-	-	-	-
	0.09**	0.15**	0.24**	-0.2**

Table 3. The changes in probability of poor visibility, $p(V|X) - p(V)$, due to the impact of the dynamical variable X as defined in the text. Visibility observations and NCEP-NCAR reanalysis data have been used for this computation.

Quantity X	Nov.	Dec.	Jan.	Feb.
SFI	7	-8	4	-4
B	19	16	2	11
K	-1	-1	2	-10
K_{mf}	0	-1	2	-7
K_s	0	6	-8	-4
MF	5	3	-5	-2
S	-4	1	4	1
F_{high}	5	9	11	4
F_{low}	-6	-14	-14	-16

3.2. The role of surface pressure systems

In the long-term study at Mehrabad Airport, a decreasing trend is observed for each of the 90th (“poor”), 50th (“median”) and 10th (“good”) percentiles of the visibility. The trends seen for the good, poor and median visibilities in the filtered data are steeper than those in the raw data. Among these three cumulative percentiles, the steepest slope belongs to the good visibility of the filtered data, next to which is the median, with the smallest slope being that of the poor visibility (Figure 1).

During the long-term period, the decreasing trend seen in the poor filtered visibility is higher than that of the poor visibility based on the raw data. This indicates that the surface meteorological factors accounted for in filtering have had a positive impact on the visibility. The same statement holds

true for the median and good visibilities. However, since the mid-1980s, the trends of the median and good visibilities of the raw data are above the trends of the filtered visibilities, showing that in the last three decades, the effects of degradation in air quality have been felt more strongly in the good and median visibilities.

Figure 2 illustrates the 56 year average frequency of occurrence for both the high and low surface pressure systems for the extended winter, or cold half of year, from October to April. During the whole period, the frequencies of occurrence are greater for the high-pressure systems and the high-to-low ratio peaks in October and takes its lowest value in March. There seems to be a phase difference in the oscillatory behavior of the low- and high-pressure frequencies of occurrence. The phase difference is such that while for the high pressure, one can see three maxima in October, January and March, for the low pressure, there are two maxima, a flat maximum in November and December and a sharper in March.

The time series of the frequencies of occurrence for both high- and low-pressure systems during winter season, taken to include December, January and February, have been depicted in Figure 3 separately for the periods 1958–2013 and 1983–2013. The presence of an increasing trend for the high-pressure and a decreasing trend for the low-pressure systems during winter season is apparent. The effect is such that the dominance of the low-pressure systems over the first 10 to 15 years of the period has been replaced by the dominance of the high-pressure systems over the last 20 years of the period. Further, on average for the whole period, the high-to-low ratio has become $25/14 \approx 1.8$. The decreasing trend seen for the low-pressure systems during the whole period is, however, absent or replaced by a slight increasing trend during the last thirty years of the record.

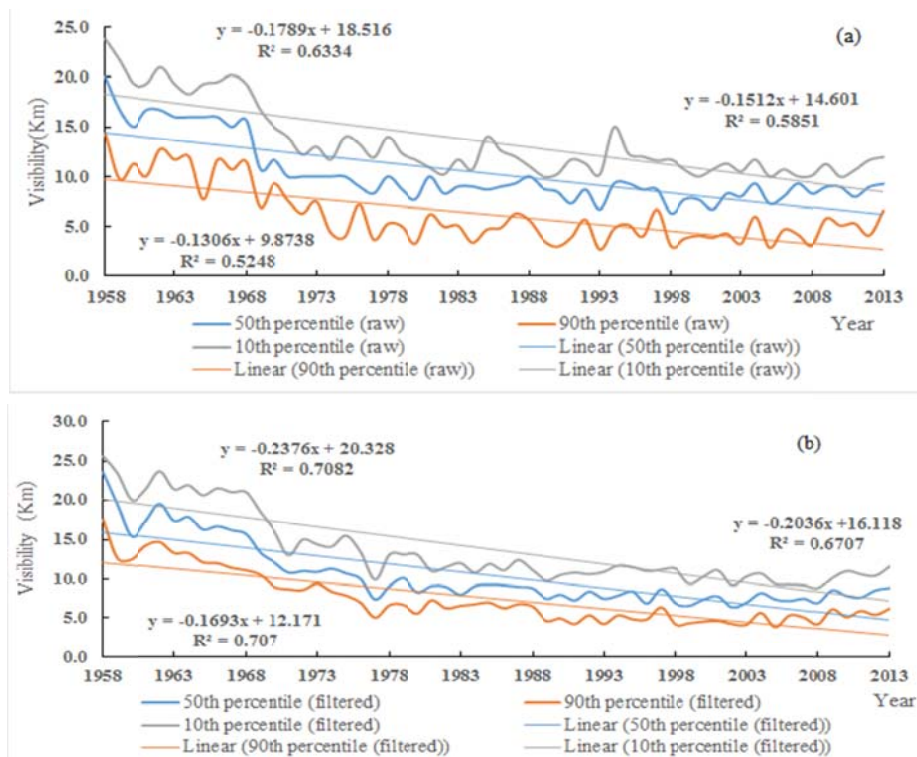


Figure 1. Time series of the 90th (brown), 50th (blue) and 10th (gray) percentiles of (a) raw and (b) filtered visibility observations in Mehrabad airport station during 1958–2013 period. The straight lines are for the corresponding linear trends.

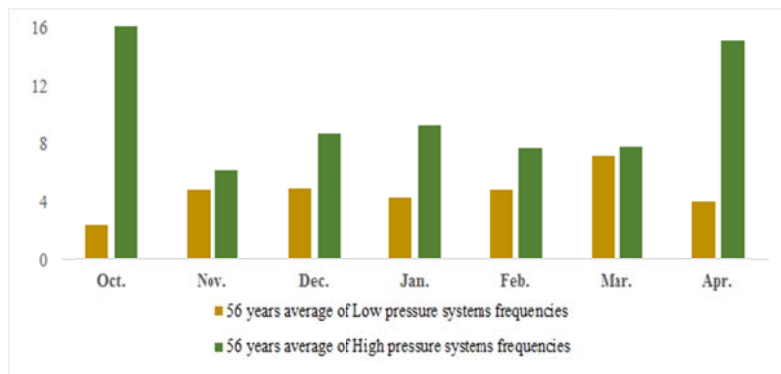


Figure 2. Monthly averages of the low (orange) and high (green) mean sea level pressure systems in 34–37° N, 48–54° E during 1958–2013, based on sea level pressure data from the NCEP-NCAR reanalysis dataset.

The correlation values of the 10th, 50th and 90th percentiles of both raw and filtered visibilities with the frequencies of occurrence of high/low surface pressure systems computed for the whole period have been given in Table 4. All the correlations in Table 4 are significant at 0.01 level. While the negative correlations seen for the high-pressure frequency of occurrence is a clear indication of the degrading effect of the

high-pressure disturbances on the visibility, the positive values for the low-pressure frequencies can be attributed to the ventilating effect of low pressure systems. It is also interesting that, at each percentile, the relation between the visibility and the surface pressure systems is stronger for the low pressure systems. This can be interpreted as the criticality of ventilation by low-pressure systems for the improvement in visibility and thus air quality in Tehran.

Table 4. The correlation values between high/low surface pressure systems frequencies of occurrence (obtained from sea level pressure data of the NCEP-NCAR reanalysis dataset) and the filtered/raw visibility percentiles in DJF during 1958–2013.

DJF-56 years	50 th percentile (filtered)	90 th percentile (filtered)	10 th percentile (filtered)	50 th percentile (raw)	90 th percentile (raw)	10 th percentile (raw)
high-pressure	-0.55	-0.55	-0.56	-0.50	-0.55	-0.49
low-pressure	0.73	0.73	0.72	0.71	0.69	0.71

To gain more insight to the relation between the visibility percentiles and pressure systems, the correlation values have been computed between the number of days for which the visibility is under the threshold given by Equation (5) and the frequencies of occurrence of high/low pressure systems. The results for the filtered visibility and the winter months are given in Table 5. All the correlations are significant at 0.05 level. It is

important to note the change in sign of correlations with respect to the values given in Table 4. In addition to this sign change, which is expected, the differences in correlation values for the high- and low-pressure systems are generally closer than those in Table 4. That is, there is less difference in the effect of the high- and low-pressure systems as regards the number of cases of poor visibility.

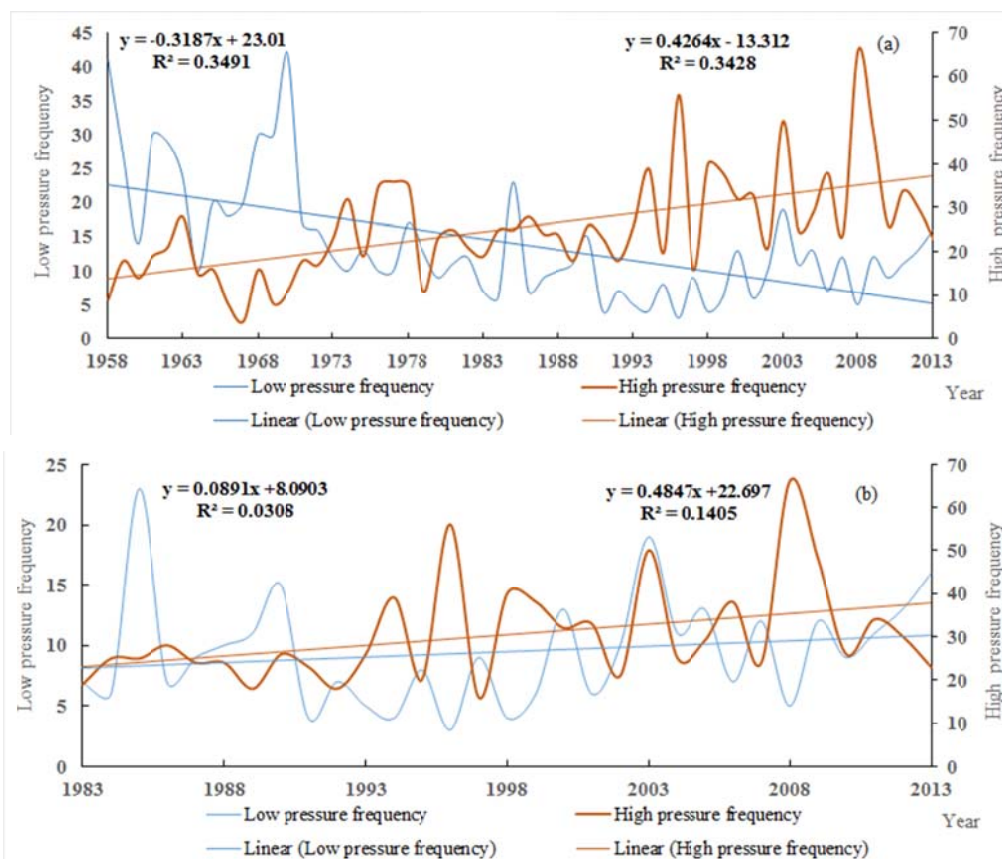


Figure 3. Time series of frequencies of occurrence of high (blue) and low (brown) pressure systems in DJF months for (a) 1958–2013 and (b) 1983–2013 period, based on the sea level pressure data of the NCEP-NCAR reanalysis dataset. The straight lines are for the corresponding linear trends.

Table 5. The correlation values between the frequencies of high/low surface pressure systems (based on the sea level pressure data of the NCEP-NCAR reanalysis dataset) and the poor visibility based on the filtered visibility data from Mehrabad Airport synoptic station for Dec., Jan., and Feb. months during 1958–2013.

	Dec.	Jan.	Feb.
high-pressure versus visibility	0.53	0.35	0.35
low-pressure versus visibility	-0.46	-0.52	-0.42

4. Conclusions

Given the acute air pollution episodes during cold seasons in Tehran metropolitan in recent decades, the key motivation for this work was to find the relations between the visibility as one of the good indicators of air quality and dynamical phenomena of large to meso scales including jet splitting, blocking, and high and low surface pressure systems. Finding such relations is of prime importance as it can help us understand the impacts of climate change in the coming decades on air quality in the megacity of Tehran.

To this end, two main types of data were used. The visibility observations in three-hourly intervals were provided from Tehran Mehrabad Airport synoptic station for the period 1958–2013. From NCEP/NCAR reanalysis data, the sea surface pressure, zonal and meridional wind and air temperature were obtained for the same period in six hourly intervals. To eliminate the effect of weather conditions on visual range, the visibility dataset was screened by removing cases of fog, precipitation of any kind and relative humidity above 70%. For both the unscreened and screened visibility, the daily mean values and the percentiles of good, median and poor visibility were obtained. By moving from the upper levels of troposphere to the lower levels and applying several dynamical indices, an extensive search was made for any robust relation between the dynamical phenomena and the visibility impairment. The split flow index (SFI) as a measure of the strength and location of the two main jet streams as well

as the inactive gap region between the two jets was determined for the Tehran region. The B index for Rossby wave breaking based on the reversal of the meridional gradient of potential temperature at the 2PVU surface, the eddy kinetic energy for synoptic-scale eddies with and without multiplication by the sign of meridional momentum flux or static stability was also considered. To provide a uniform framework for the interpretation of the results for the dynamical indices, it was important to categorize the indices properly. Visibility observations were de-trended in order to make them consistent with the dynamical indices, which showed no definite trend during the climatological period. The chi-squared test of independence, the correlation estimates for daily averages, and the conditional probabilities showed no or very weak statistical relation between the visibility in Tehran and each of the SFI, the B index, the lower-tropospheric eddy kinetic energy and meridional momentum flux. There were indications of stronger relations with the lower-tropospheric static stability and to a lesser extent eddy kinetic energy when multiplied by the negative static stability, i.e. static instability.

The long-term meteorologically screened data of visibility at Mehrabad synoptic station exhibit the influence of surface weather on decreasing trend of visibility. In this respect, our results are consistent with those of Dharshana et al. (2010) for the US. Our conditional probability estimates of poor visibility indicate that only up to about 15% and 10% of the increase in cases of poor visibility can be attributed to, respectively decrease and increase in the frequency of occurrence of the low and high surface pressure systems. For all cumulative percentiles, the correlation between the visibility and the frequency of occurrence of high and low surface pressure systems is estimated at about -0.5 and 0.7, respectively. There is little difference in estimates of correlation for the filtered and raw observations.

The tropospheric processes are definitely involved in the ventilation and accumulation processes as the case studies of acute air-pollution episodes show. However, as our results suggest, establishing a robust relation between the large-scale dynamical indices,

especially those related to upper-tropospheric processes, and the air pollution or visibility impairment happening in boundary layer has proved elusive in this region. The main reason may be the slow response of the urban ventilation and accumulation processes to the faster time evolution at upper levels of the troposphere. The slow response may be a result of complex terrain (Bell and Thompson, 1980) exacerbated by the effects of fast population growth, ever-increasing levels of population concentration, as well as the rapid growth in the car use and housing projects. On the other hand, the surface related factors such as the occurrence of high/low surface pressure systems exhibit rather well-defined relations with visibility degradation.

Acknowledgments

We would like to thank the University of Tehran for providing support during this research.

References

- Adams, J. C. and Swartztrauber, P. N., 1999, SPHEREPACK 3.0: A model development facility. *Monthly Weather Review*, 127, 1872–1878.
- Bals-Elsholz, T., Atallah, E., Bosart, L., Wasula, T., Cempa, M. and Lupo, A., 2001, The wintertime Southern Hemisphere split jet: Structure, variability, and evolution. *Journal of Climate*, 14, 4191–4215.
- Baumer, D., Vogel, B., Versick, S., Rinke, R., Mohler, O. and Schnaiter, M., 2008, Relationship of visibility, aerosol optical thickness and aerosol size distribution in an ageing air mass over South-West Germany. *Atmospheric Environment*, 42, 989–998.
- Bell, R.C. and Thompson, R.O.R.Y., 1980, Valley ventilation by cross winds. *Journal of Fluid Mechanics*, 96, 757–767.
- Chang, D., Song, Y. and Liu, B., 2009, Visibility trends in six megacities in China 1973–2007. *Atmospheric Environment*, 43, 161–167.
- Chang, E. K. M., Lee, S. and Swanson, K. L., 2002, Storm track dynamics. *Journal of Climate*, 15, 2163–2183.
- Cooper, O., Moody, J., Parrish, D., Trainer, M., Holloway, J., Ryerson, T., Hubler, G., Fehsenfeld, F., Oltmans, S. and Evans, M., 2001, Trace gas signatures of the airstreams within North Atlantic cyclones: case studies from the North Atlantic Regional Experiment (NARE'97) aircraft intensive. *Journal of Geophysical Research*, 106, 5437–5456.
- Craig, C. D. and Faulkenberry, G. D., 1979, The application of ridit analysis to detect trends in visibility. *Atmospheric Environment*, 13, 1617–1622.
- Dagsson-Waldhauserova, P., Arnalds, O. and Olafsson, H., 2013, Long-term frequency and characteristics of dust storm events in Northeast Iceland (1949–2011). *Atmospheric Environment*, 77, 117–127.
- Demuzere, M., Trigo, R. M., Arellano, J. V. and van Lipzig, N. P. M., 2009, The impact of weather and atmospheric circulation on O₃ and PM₁₀ levels at a rural mid-latitude site. *Atmos. Chem. Phys.*, 9, 2695–2714.
- Deng, J., Du, K., Wang, K., Yuan, C. and Zhao, J., 2012, Long-term atmospheric visibility trend in Southeast China, 1973–2010. *Atmospheric Environment*, 59, 11–21.
- Deng, X., Tie, X., Wu, D., Zhou, X., Bi, X., Tan, H., Li, F. and Jiang, C., 2008, Long-term trend of visibility and its characterizations in the Pearl River Delta (PRD) region, China. *Atmospheric Environment*, 42, 1424–1435.
- Dharshana, K. G. T., Kravtsov, S. and Kahl, J.D.W., 2010, Relationship between synoptic weather disturbances and particulate matter air pollution over the United States. *Journal of Geophysical Research*, 115, D24219.
- Doyle, M. and Dorling, S., 2002, Visibility trends in the UK 1950–1997. *Atmospheric Environment*, 36, 3161–3172.
- Duchon, C. E., 1979, Lanczos filter in one and two dimensions. *Journal of Applied Meteorology*, 18, 1016–1022.
- Forkel, R. and Knoche, R., 2006, Regional climate change and its impact on photo oxidant concentrations in southern Germany: Simulations with a coupled regional chemistry–climate model. *Journal of Geophysical Research*, 111, D12302.
- Gultepe, I. and Milbrandt, J., 2009, Probabilistic parameterizations of

- visibility using observations of rain, precipitation rate, relative humidity, and visibility. *Journal of Applied Meteorology and Climatology*, 49, 34–46.
- Hafezi, M., Rezaeimanesh, M., Mohebalhojeh, A., Bidokhti, A. A. and Nasr- Esfahany, M., 2015, Application of the split flow and Rossby-wave breaking indices to study critical air pollution episodes in Tehran during Nov. and Dec. 2010. *Iranian Journal of Geophysics*, 9, 134–149.
- Haynes, P. and McIntyre, M., 1987, On the evolution of vorticity and potential vorticity in the presence of diabatic heating and other forces. *Journal of the Atmospheric Sciences*, 44, 828–841.
- Hoskins, B., McIntyre, M. and Robertson, A., 1985, On the use and significance of isentropic potential vorticity maps. *Quarterly Journal of the Royal Meteorological Society*, 111, 877–946.
- Husar, R. B., Holloway, J. M., Poll, D. E. and Wilson, W. E., 1981, Spatial and temporal pattern of eastern US haziness: a summary. *Atmospheric Environment*, 15, 1919–1928.
- Kalnay, E., Kanamitsu, M., Kistler, R., Collins, W., Deaven, D., Gandin, L., Iredell, M., Saha, S., White, G., Woollen, J., Zhu, Y., Leetmaa, A., Reynolds, B., Chelliah, M., Ebisuzaki, W., Higgins, W., Janowiak, J., Mo, K. C., Ropelewski, C., Wang, J., Jenne, R. and Joseph, D., 1996, The ncep/ncar 40-year reanalysis project. *Bulletin of the American Meteorological Society*, 77, 437–472.
- Lambert, S. and Fyfe, J., 2006, Changes in winter cyclone frequencies and strengths simulated in enhanced greenhouse warming experiments: results from the models participating in the IPCC diagnostic exercise. *Climate Dynamics*, 26, 713–728.
- Leibensperger, E., Mickley, L. and Jacob, D., 2008, Sensitivity of U.S. air quality to midlatitude cyclone frequency and implications of 1980–2006 climate change. *Atmospheric Chemistry and Physics*, 8, 7075–7086.
- Li, Q., Jacob, D., Park, R., Wang, Y., Heald, C., Hudman, R., Yantosca, R., Martin, R. and Evans, M., 2005, North American pollution outflow and the trapping of convectively lifted pollution by upper-level anticyclone. *Journal of Geophysical Research*, 110, D10301.
- Liao, W., Wang, X., Fan, Q., Zhou, S., Chang, M., Wang, Z., Wang, Y. and Tu, Q., 2015, Long-term atmospheric visibility, sunshine duration and precipitation trends in South China. *Atmospheric Environment*, 107, 204–216.
- Liu, H., Jacob, D. J., Bey, I., Yantosca, R. M., Duncan, B. N. and Sachse, G. W., 2003, Transport pathways for Asian combustion outflow over the Pacific: Interannual and seasonal variations. *Journal of Geophysical Research*, 108, D20.
- Malm, W. C. and Day, D. E., 2001, Estimates of aerosol species scattering characteristics as a function of relative humidity. *Atmospheric Environment*, 35, 2845–2860.
- Meehl, G. A., Stocker, T. F., Collins, W. D., Friedlingstein, P., Gaye, A. T., Gregory, J. M., Kitoh, A., Knutti, R., Murphy, J. M., Noda, A., Raper, S. B., Watterson, I. G., Weaver, A. J. and Zhao, Z. C., 2007, Global climate projections. In: Solomon, S., Qin, D., Manning, M., Chen, Z., Marquis, M., Averyt, K., Tignor, M., Miller, H.L. (Eds.), *Climate Change 2007: The Physical Science Basis*, Cambridge University Press, 747–846.
- Mickley, L. J., Jacob, D. J., Field, B. D. and Rind, D., 2004, Effects of future climate change on regional air pollution episodes in the United States. *Geophysical Research Letters*, 30, L24103.
- Molenar, A., Meszaros, E., Imre, K. and Rull, A., 2008, Trends in visibility over Hungary between 1996 and 2002. *Atmospheric Environment*, 42, 2621–2629.
- Murazaki, K. and Hess, P., 2006, How does climate change contribute to surface ozone change over the United States? *Journal of Geophysical Research*, 111, D05301.
- Ordóñez, C., Mathis, H., Furger, M., Henne, S., Hoglin, C., Staehelin, J. and Prevot, A. S. H., 2005, Changes of daily surface ozone maxima in Switzerland in all seasons from 1992 to 2002 and discussion of summer 2003. *Atmospheric Chemistry and Physics*, 5, 1187–1203.

- Pearce, J. L., Beringer, J., Nicholls, N., Hyndman, R. J. and Tapper, N. J., 2011, Quantifying the influence of local meteorology on air quality using generalized additive models. *Atmospheric Environment*, 45, 1328–1336.
- Pelly, J. and Hoskins, B. J., 2003, A new perspective on blocking. *Journal of the Atmospheric Sciences*, 60, 743–755.
- Pope, R. J., Savage, N. H., Chipperfield, M. P., Arnold, S. R. and Osborn, T. J., 2014, The influence of synoptic weather regimes on UK air quality: analysis of satellite column NO₂. *Atmospheric Science Letters*, 15, 211–217.
- Pope, R. J., Savage, N. H., Chipperfield, M. P., Ordóñez, C. and Neal, L. S., 2015, The influence of synoptic weather regimes on UK air quality: regional model studies of tropospheric column NO₂. *Atmospheric Chemistry and Physics*, 15, 11201–11215.
- Pusheng, Z., Xiaoling, Z., Xiaofeng, X. and Xiujuan, Z., 2011, Long-term visibility trends and characteristics in the region of Beijing, Tianjin, and Hebei, China. *Atmospheric Research*, 101, 711–718.
- Rohli, V. R., Russo, M. M., Vega, A. J. and Cole, J. B., 2004, Tropospheric ozone in Louisiana and synoptic circulation. *J. Appl. Meteor.* 43, 1438–1451.
- Sabetghadam, S., Ahmadi-Givi, F. and Golestani, Y., 2012, Visibility trend in Tehran during 1958–2008. *Atmospheric Environment*, 35, 512–520.
- Samet, J. and Krewski, D., 2007, Health effects associated with exposure to ambient air pollution. *Journal of Toxicology and Environmental Health, Part A*, 70, 227–242.
- Seinfeld, J. H. and Pandis, S. N., 2006, *Atmospheric Chemistry and Physics: From Air Pollution to Climate Change*, 2nd Edition. Wiley-Interscience.
- Shen, L. and Mickley, L. J., 2017, Seasonal prediction of US summertime ozone using statistical analysis of large scale climate patterns. *Journal of Geophysical Research*, 114, 2491–2496.
- Sisler, J. F. and Malm, W. C., 1994, The relative importance of soluble aerosols to spatial and seasonal trends of impaired visibility in the United States. *Atmospheric Environment*, 28, 851–862.
- Sloane, C. S., 1982a, Visibility trends — I, methods of analysis. *Atmospheric Environment*, 16, 41–51.
- Sloane, C. S., 1982b, Visibility trends—II, Mideastern United States 1948–1878. *Atmospheric Environment*, 16, 2309–2321.
- Sloane, C. S., 1984, Meteorologically adjusted air quality trends: visibility. *Atmospheric Environment*, 18, 1217–1229.
- Tai, A.P.K., Mickley, L. J., Jacob, D. J., Leibensperger, E. M., Zhang, L., Fisher, J. A. and Pye, H.O.T., 2012, Meteorological modes of variability for fine particulate matter (PM_{2.5}) air quality in the United States: implications for PM_{2.5} sensitivity to climate change. *Atmospheric Chemistry and Physics*, 12, 3131–3145.
- Thorncroft, C. D., Hoskins, B. and McIntyre, M., 1993, Two paradigms of baroclinic wave life-cycle behavior. *Quarterly Journal of the Royal Meteorological Society*, 119, 877–946.
- Webber, C. P., Dacre, H. F., Collins, W. J. and Masato, G., 2017, The dynamical impact of Rossby wave breaking upon UK PM₁₀ concentration. *Atmospheric Chemistry and Physics*, 17, 867–881.
- Wu, S., Mickley, L. J., Leibensperger, E. M., Jacob, D. J., Rind, D. and Streets, G., 2008, Effects of 2000–2050 global change on ozone air quality in the United States. *Journal of Geophysical Research*, 113, D06302.
- Xiao, S., Wang, Q. Y., Cao, J. J., Huang, R. J., Chen, W. D., Han, Y. M., Xu, H. M., Liu, S. X., Zhou, Y. Q., Wang, P., Zhang, J. Q. and Zhan, C. L., 2014, Long-term trends in visibility and impacts of aerosol composition on visibility impairment in Baoji, China. *Atmospheric Research*, 149, 88–95.